OPEN ACCESS

Chemical Engineering ARTICLE

The Innovation Materials

Ultra-low-energy CO_2 capture by planar-stacked solid amine sorbent with pulsed microwave regeneration

Yunxia Wen,[1,4] Peng Jiang,[1,4] Mingxing Zhou,[1] Han Wang,[1] Tong Zhou,[1] Zhinan Wu,[1] Bei Liu,[1] Ning Qu,[2] Jie Kong,[2] Huacheng Zhu,[3] Yang Yang,[3] Han Lin,[1] Xiaohua Lu,[1] Tuo Ji,[1,*] and Jiahua Zhu[1,*]

*Correspondence: tuoji@njtech.edu.cn (T.J.); jhzhu@njtech.edu.cn (J.Z.)

Received: October 20, 2025; Accepted: June 16, 2026; Published Online: June 16, 2026; https://doi.org/10.59717/j.xinn-mater.2026.100224

GRAPHICAL ABSTRACT

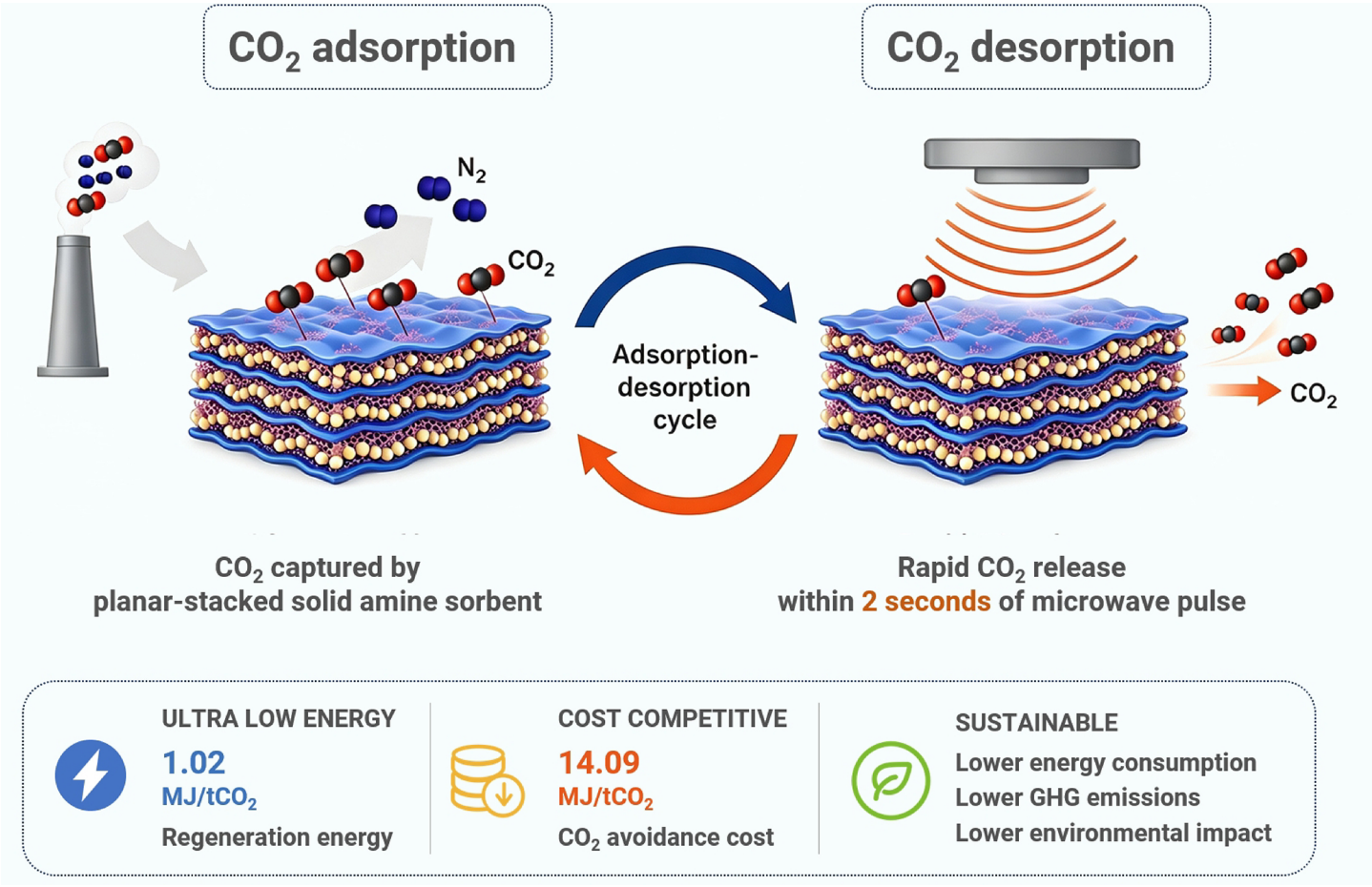

PUBLIC SUMMARY

- Microwave-responsive PEI-based solid sorbent developed for efficient CO_2 capture.
- Pulsed microwave regeneration achieves ultra-low energy use of 1.02 MJ/tCO_2.
- Techno-economic analysis shows CO_2 avoidance cost reduced to 14.09 USD/tCO_2.

ARTICLE Chemical Engineering

OPEN ACCESS

Ultra-low-energy CO_2 capture by planar-stacked solid amine sorbent with pulsed microwave regeneration

Yunxia Wen,[1,4] Peng Jiang,[1,4] Mingxing Zhou,[1] Han Wang,[1] Tong Zhou,[1] Zhinan Wu,[1] Bei Liu,[1] Ning Qu,[2] Jie Kong,[2] Huacheng Zhu,[3] Yang Yang,[3] Han Lin,[1] Xiaohua Lu,[1] Tuo Ji,[1,*] and Jiahua Zhu[1,*]

[1]State Key Laboratory of Material-Oriented Chemical Engineering, College of Chemical Engineering, Nanjing Tech University, Nanjing 211816, China

[2]School of Chemistry and Chemical Engineering, Northwestern Polytechnical University, Xi'an 710129, China

[3]College of Electronics and Information Engineering, Sichuan University, Chengdu 610065, China

[4]These authors contributed equally

*Correspondence: tuoji@njtech.edu.cn (T.J.); jhzhu@njtech.edu.cn (J.Z.)

Received: October 20, 2025; Accepted: June 16, 2026; Published Online: June 16, 2026; https://doi.org/10.59717/j.xinn-mater.2026.100224

Citation: Wen Y., Jiang P., Zhou M., et al. (2026). Ultra-low-energy CO_2 capture by planar-stacked solid amine sorbent with pulsed microwave regeneration. *The Innovation Materials* **4**:100224.

Carbon dioxide (CO_2) capture with energy duty of below 2.0 MJ·kg^{-1} CO_2 is the global prospect in the decarbonization process. Herein, we present a microwave-responsive amine sorbent coupled with a pulsed microwave regeneration (AS-MR) process that achieves rapid and fully regeneration of amine sorbent within 2 seconds of microwave pulse. By matching the energy input with the desorption rate, ultra-low energy duty of 1.02 MJ·kg^{-1} CO_2 can be achieved for sorbent regeneration and 1.21 MJ·kg^{-1} CO_2 for the AS-MR system during an adsorption-desorption cycle. Insights into the mechanism indicate that the directional electric field aids the CO_2 desorption process by weakening and polarizing the C-N bond in the carbamate acid state. Techno-economic analysis and life cycle assessment demonstrate the sustainability of this technology with costs below $20·tonne^{-1}, directly responding to the pressing demand for economically viable decarbonization technologies in challenging industrial sectors.

INTRODUCTION

Capturing carbon dioxide (CO_2) from industrial processes has been recognized as the primary driver for governing global warming.[1,2] The Intergovernmental Panel on Climate Change (IPCC) suggested a new target in 2018, seeking to limit global warming to 1.5 °C above pre-industrial levels.[3] Amine scrubbing has been scaled up and practiced in industry to capture CO_2 (10~15%) from flue gases.[4,5] However, it comes with a high energy penalty during regeneration and fails to meet the next-generation energy goal of 2.0 MJ·kg^{-1}-CO_2.[6] Also, issues like equipment corrosion,[7] and handling of the spent amine solution make it expensive to capture CO_2, i.e., 50-90 USD·tonne^{-1} CO_2.[8,9] Therefore, transformational technologies are demanded to capture CO_2 with low energy duty and low cost.

One attractive strategy is to develop solid sorbents by immobilizing amines on supports.[10,11] The main advantage of solid sorbents is water-free, avoiding the huge energy consumption during evaporation (for regeneration) and potentially reducing the overall costs.[12] To achieve high working capacity and fast mass transfer, sorbent is often designed to have high amine loading ratio of beyond 50 wt%, meanwhile, soft packing of amine structure for efficient CO_2 diffusion and adsorption. These two requirements make sorbents bad thermal conductors, thus generating temperature gradient and uneven CO_2 desorption across external to internal surfaces.[13,14] To realize full regeneration, overly long heating time is often needed, resulting in sorbent degradation and excessive energy consumption. Therefore, it remains a challenge to design solid sorbents with a large CO_2 adsorption capacity while still capable of conducting heat effectively.

Microwave heating is well known for its uniform heating and fast heating rates[15] which has been used in the regeneration process of solvent-based[16,17] and sorbent-based[18] CO_2 capture systems. Yang et al.[19] used perfluorinated silica-stabilized dry alkanolamines for CO_2 capture and applied microwave for regeneration. Results indicated a dramatic reduction of energy consumption from 0.38 kWh per cycle to 0.034 kWh per cycle by switching from conventional heating to microwave heating. However, in reported microwave-involved cases, energy consumption is still relatively high. For instance, Bougie et al.[16] investigated the microwave regeneration of aqueous monoethanolamine (MEA) solutions for CO_2 capture, reporting a desorption energy consumption as high as 40 GJ·t^{-1}-CO_2. Similarly, Erguvan et al.[20] studied microwave-assisted CO_2 desorption from solid sorbents in a fluidized-bed reactor, yet the energy consumption still reached 35 GJ·t^{-1}-CO_2. Overseeing these processes, the microwave system is far from optimization since it lacks effective design on both material and device structures. Majority of the amine sorbents used SiO_2 or zeolite supports, which are microwave transparent and has no function to attract microwave energy. In addition, most microwave devices are not designed to regenerate sorbent so the way of energy delivery and system integration are still under development.

In this work, an amine sorbent-microwave regeneration (AS-MR) system was developed to capture CO_2 with ultra-low energy duty. Specifically, the AS-MR system comprised a microwave desorption unit and a planar-stacked microwave-responsive sorbent (Figures 1A-B), both enabling synergistic and targeted energy delivery (Figure 1C). This design achieved complete sorbent regeneration within 2 seconds of microwave pulsing. An ultra-low energy duty of 1.02 MJ·kg^{-1} CO_2 was required for sorbent regeneration, and 1.21 MJ·kg^{-1} CO_2 for the entire AS-MR cycle (Figure 1D). The synergistic mechanism between microwave irradiation and the sorbent lies in the polarity difference of the sorbent before and after CO_2 adsorption, which induces selective and efficient microwave energy absorption (Figure 1E). Subsequently, techno-economic analysis (TEA) and life cycle assessment (LCA) were conducted for the AS-MR system, revealing a remarkably low CO_2 avoidance cost of only 14.09 USD·tonne^{-1} CO_2. Looking forward, with the advancement of green electricity, microwave-driven carbon capture technology featuring ultrafast kinetics and ultra-low energy consumption offers a transformative solution for large-scale CO_2 mitigation (Figure 1F).

MATERIALS AND METHODS

Preparation of polyethyleneimine-graphene oxide@silica (PEI-GS)

Graphene oxide (GO) powder was dispersed in a 130 mL ethanol aqueous solution, maintaining an ethanol/H_2O ratio of 25:1, and underwent sonication for 30 min. Then, 5.0 g of TEOS and 5.0 g ammonia aqueous solution was dropwise added into the mixture while continuously stirring. Upon completion of the dropping process, the degree of hydrolysis was evaluated by monitoring the electrical conductivity of the resultant suspension until it stabilized, typically within 10-12 h. The mixture was centrifuged and the resulting solid was then washed with methanol solution. This process was repeated twice, ultimately obtaining GS nanocomposites. To study the effect of GO@SiO_2 ratio on polyethyleneimine (PEI) loading, five GS samples with varying ratios were prepared and named GS3, GS5, GS7, GS10, and GS15 according to actual GO content in the sample, respectively.

The PEI sorbents were synthesized through the impregnation method.[21] A certain ratio of PEI and GS composite was added to 20.0 g of methanol. After thorough mixing, the mixture was transferred to a 100 mL round flask on a rotary evaporator and heated at a temperature of 60°C. The vacuum pressure gradually decreased to -0.05 MPa in the first 20 min to ensure that the solvent did not boil. After 60 min, the solvent completely evaporated, and the obtained solid was named PEI10-GS, PEI20-GS, PEI30-GS, PEI40-GS, and PEI50-GS according to the PEI loading (10%, 20%, 30%, 40%, and 50%, respectively).

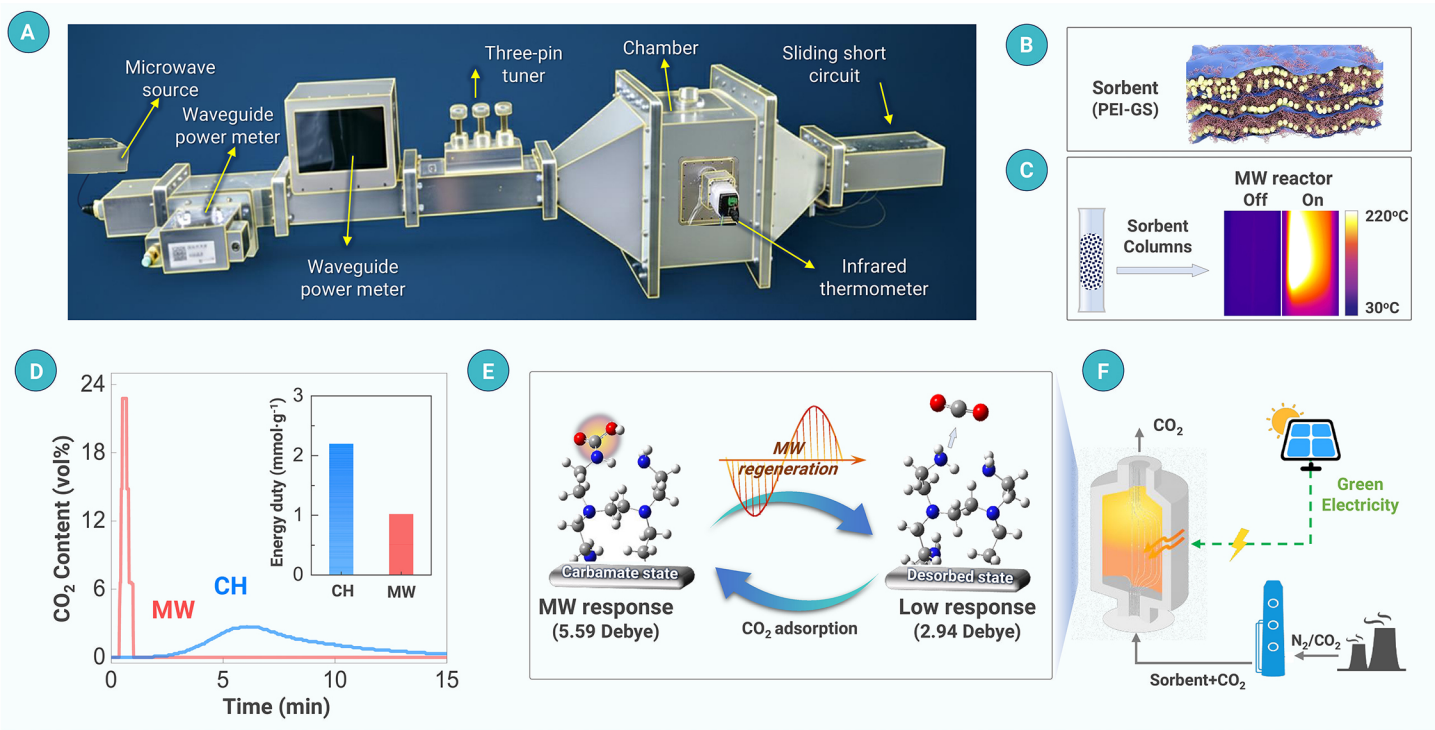

Figure 1. Planar-stacked microwave-responsive sorbents enable rapid and energy-efficient CO_2 regeneration in the AS–MR system (A) Photo of microwave regeneration devices for the AS-MR system (B) Planar-stacked structure of the microwave-responsive adsorbent. (C) Photo and IR-camera photo of sorbent beds under microwave irradiation; (D) Comparison of CO_2 release kinetics and energy consumption of Polyethylenimine-Graphene Oxide@Silica (PEI-GS) sorbents with microwave (MW) and conventional heating (CH). (E) Microwave regeneration mechanism of adsorbent, and (F) conceptual diagram of using green electricity to remove CO_2 from flue gas via AS-MR system.

Microwave-assisted CO_2 adsorption-desorption test

The experimental setup involved meticulously placing 0.1 g of the sample within a quartz U-tube positioned within the chamber. Thermocouples were strategically positioned to monitor the bed temperature in real time, ensuring precise control throughout the experiment. The gas flow was directed through the U-tube following its passage through two calibrated mass flow controllers. A CO_2 detector was meticulously attached to the exit gas flow from the reactor, allowing for accurate measurements of CO_2 adsorption. Each experiment was conducted under atmospheric pressure, and all gas lines were meticulously purged with N_2 both before and after the experimental runs to prevent any unintentional CO_2 adsorption by the sorbents. A bypass line with a three-way valve was installed in the fixed-bed setup to switch between CO_2 adsorption (14 vol% CO_2/N_2) and N_2 purge for regeneration, maintaining stable reactor pressure and temperature. This ensured reliable CO_2 capture measurements at 60°C.

The CO_2 capture performance of sorbent was evaluated by adsorption at 60°C (the temperature of flue gas) and microwave regeneration process. Before CO_2 adsorption, 0.1 g sorbent was packed into the quartz tube and maintained at 105°C under 100 mL·min^{-1} N_2 atmosphere for 15 min. Then the temperature dropped to 60°C for CO_2 adsorption. Once the temperature stabilized, the gas flow was switched to a mixture of 14 mL·min^{-1} CO_2 and 86 mL·min^{-1} N_2 and held for 30 min for CO_2 adsorption.

Before microwave irradiation, the sorbent was purged with N_2 to remove any physically adsorbed CO_2. After microwave irradiation, 100 mL·min^{-1} N_2 flow was switched back to purge the gas lines and then acted as a sweeping gas. The microwave power and irradiation time were controlled, respectively, to study their effect on sorbent regeneration. The amount of desorbed CO_2 was measured by an IR gas sensor (K23E35). The waveguide power meter measured the forward and reflected microwave power and the difference between them represented the amount of energy absorbed by the solid sorbents. The amount of stripped CO_2 was determined by direct integration of the outlet CO_2 concentration which was measured by IR CO_2 sensor.

Characterization

The crystal structure of materials was analyzed using a Bruker AXSD8 Advance X-ray diffractometer (XRD) with Cu Kα radiation, a working voltage of 40 kV, a current of 100 mA, a scanning range of 10-90°, a scanning speed of 0.5°·min^{-1}, and a step size of 0.02°. The Raman analysis was carried out on a Horiba HR800 Raman spectrometer in which the wavenumber of the Ar^+ laser was set as 514.5 nm. The specific surface areas of catalysts were determined through N_2 adsorption/desorption isotherms collected on a Micromeritics Tristar II 3020. The surface morphology of the material was observed using a HITACHI S-4800 scanning electron microscope (SEM). The microstructure and morphology of sorbents were characterized by transmission electron microscopy (TEM, JEM 2100F). Rigaku ZSX-Primus II type X-ray photoelectron spectroscopy (XPS) was used to determine the surface composition, surface metal valence, and electronic status of the sorbents. The Thermo Nicolet 8700 Fourier Transform Infrared Spectrometer (FT-IR) was used to analyze the functional groups and chemical bonds of materials. CO_2 adsorption capacity was measured using Thermogravimetric analysis (TG, SDT650) with a temperature accuracy of ± 0.1°C and a mass accuracy of ± 0.001 mg. Vector network analyzer (VNA, MS4644A, Anritsu, Atsugi, Japan) was used to measure the dielectric properties of materials.

Computational section

All geometry structures of PEI-CO_2 in the chemisorbed carbamate acid (CA), transition state (TS), and physisorbed CO_2 state (PA) were fully optimized using the density functional theory (DFT) framework implemented in Gaussian 16.[22] The Becke three-parameter hybrid functional (B3LYP)[23] was employed as the exchange-correlation functional, with Grimme's D3 dispersion correction[24] included to account for weak intermolecular interactions, as implemented in Gaussian 16.[22] For all non-metal atoms, the 6-31G(d) basis set[25] with a single polarization function was used. Three categories of calculations were conducted to characterize the reaction pathways: geometry optimizations, TS optimizations, and single-point energy calculations. Geometry optimizations were performed to determine the minimum-energy structures and relative energies of reactants, intermediates, and products involved in the adsorption mechanism. Transition states were located using Berry's Optimization-Based (BOB) method and confirmed by frequency calculations.

Subsequent to optimizations, key geometric parameters were extracted from the optimized structures, including bond lengths, bond angles, and dihedral angles for carbon and nitrogen atoms. Quantum chemical descriptors

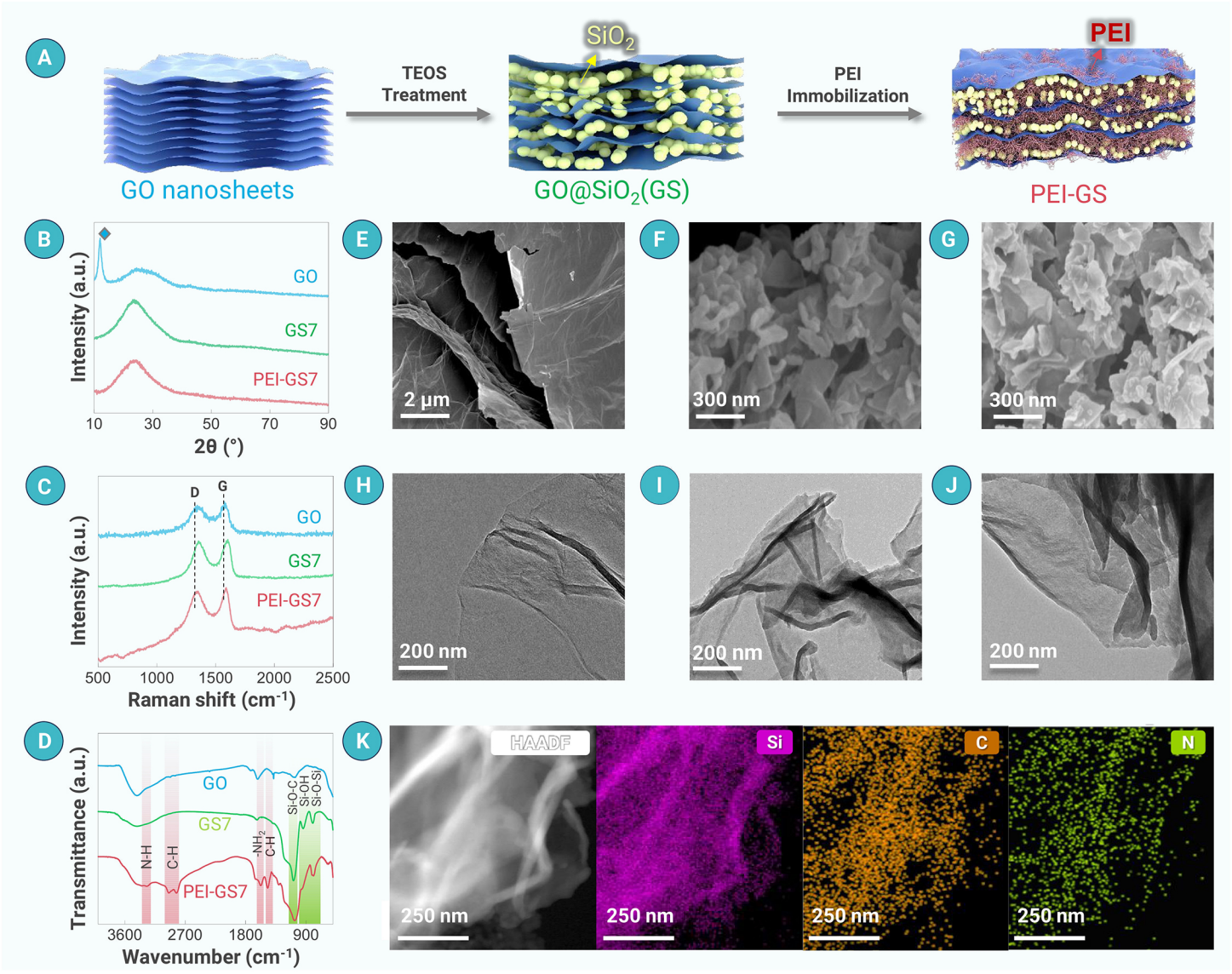

Figure 2. Catalyst characterization (A) Schematic synthesis of PEI-GS; (B) XRD spectra; (C) Raman spectra; (D) FTIR spectra; (E-G) SEM images and (H-J) HRTEM images of GO, GS7, PEI50-GS7; (K) EDX elemental mapping of PEI50-GS7.

were also analyzed, including atomic charges calculated via Mulliken population analysis method, highest occupied molecular orbital (HOMO) and lowest unoccupied molecular orbital (LUMO) energies, electron localization function (ELF) distributions, and dipole moments. Zero-point energy (ZPE) corrections were included for relative energy comparisons where applicable.

Techno-economic analysis and life cycle assessment

To analyze the advantages of microwave-responsive solid amine technology from a systemic perspective, this study established three CO_2 capture technologies: Scenario 1: Conventional MEA-based solvent capture process with thermal-driven regeneration (MEA-TSA process); Scenario 2: Solid amine capture process coupled with thermal-driven regeneration (AS-TSA process); Scenario 3: Solid amine capture process coupled with microwave-driven regeneration (AS-MR process). All three processes were evaluated with a CO_2 concentration of 14% in the flue gas and a CO_2 capture capacity of 100000 tonnes per year.

A systematic comparative analysis of CO_2 capture energy consumption, LCA, and TEA was conducted for the three technologies. The LCA methodology employed global warming potential (GWP) as an indicator to quantify carbon emission impacts. The objective was to compare the GWP associated with capturing 1 kg of CO_2 from flue gas emissions, following Equations (S5-S6) in the SI. The system boundary for the CO_2 capture LCA encompasses utility inputs and material consumption. The factored estimate method was employed for the techno-economic analysis (TEA).[26] This approach began with calculating the process plant cost (PCC) using the Aspen Process Economics Analyzer (APEA). The PCC was then used to determine the total capital requirement (TCR), total annual cost (TAC), and annual operation and maintenance cost (CO&M). The CO2-avoidance costs were calculated using equation (S7). Additionally, the cost of equipment not evaluated through the APEA module in the MW system was estimated using equations (S8).[27]

RESULTS AND DISCUSSION

Microstructure of microwave-responsive amine sorbent

We started with the synthesis of PEI/Graphene oxide@SiO_2 (PEI-GS) via TEOS treatment followed by PEI immobilization (Figure 2A). Specifically, TEOS molecules first diffused into the interlayer of GO sheets and reacted with surface hydroxyl groups, then hydrolyzed to form a layer of amorphous SiO_2. Details of TEOS surface coating, GO exfoliation, structure evolution, and subsequent PEI loading can be found in the Supporting Information for details. We then performed the XRD analysis (Figure 2B), where the disappearance of the diffraction peak at 11° (the interlayer spacing of GO[28]) in GS7 and PEI-GS7 indicated a loss of long-range order. This observation was further supported by Raman spectroscopy (Figure 2C), which showed a decrease in the G/D band intensity ratio (from 1.12 to 0.86), signifying

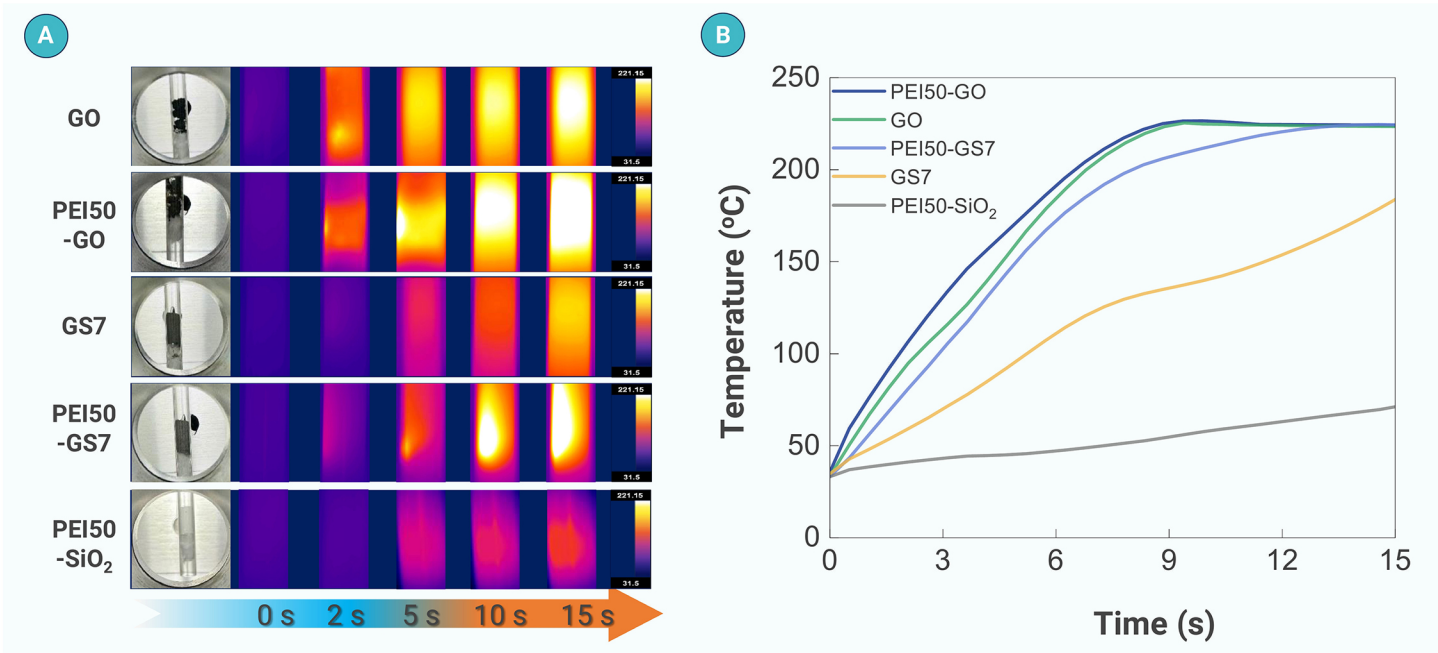

Figure 3. Microwave heating performance analysis (A) Thermal images of GO, PEI50-GO, GS7, PEI50-GS7, and PEI50-SiO_2 under 10 W microwave irradiation. (B) Temperature profile of GO, PEI50-GO, GS7, PEI50-GS7, and PEI50-SiO_2 under 10 W microwave irradiation for 15 s.

increased structural disorder. The TEOS-induced exfoliation disrupted the interlayer π-π stacking of GO, creating additional edge defects that enhanced the D-band. This spectral change, together with the loss of long-range order noted in XRD, collectively confirmed the exfoliation of GO sheets.

We conducted the FT-IR analysis (Figure 2D), which confirmed the interfacial reaction between TEOS and GO sheets as evidenced by the emerged peaks at 1088, 946, and 807 cm^{-1} corresponding to the symmetric stretching and bending vibrations of Si-O-C/Si-O-Si, Si-OH, and Si-O-Si[29] and disappearance of the typical carbonyl peak of GO at 1730 cm^{-1}. After loading PEI on the GS support, new peaks at 1304 and 3269 cm^{-1} appeared, attributing to the stretching vibration of C-N and N-H bonds from secondary amine groups, confirming the reaction between PEI and GS substrate.

The original GO sheets displayed closely stacked lamellar structures with dimensions exceeding 10 μm (Figure 2E). After treatment with TEOS, the GO sheets were exfoliated into small pieces measuring approximately 0.4 ± 0.05 μm (Figure 2F) with a thickness of about 50 nm. Following a 50 wt% PEI loading, the thickness increased to about 80 nm (Figure 2G). HRTEM results indicated that both GS7 and PEI50-GS7 samples exhibited intact nanosheet edges and bulk continuity, ruling out localized agglomeration of either SiO_2 or PEI coatings. The spatially correlated signals for C (GO), Si (SiO_2), and N (PEI) across the nanosheets suggested a uniform coating of SiO_2 and PEI on the GO sheets (Figure 2K).

Compared with conventional PEI-loaded particulate SiO_2 sorbents that often suffer from PEI agglomeration and pore blockage,[30] TEOS-induced interlayer exfoliation of GO enables the formation of a planar-stacked nanosheet architecture stabilized by an amorphous SiO_2 framework. This open and continuous structure effectively suppresses PEI migration and aggregation, enhances accessibility of amine sites, and facilitates efficient heat and mass transfer. The CO_2 adsorption behavior of sorbents under varied operation conditions was evaluated using a continuous temperature swing adsorption (TSA) equipment (Figure S1). Results showed that the GO content (3-15 wt%) exhibits a dual influence on planar structure stability and adsorption capacity. At low GO contents (3-7 wt%), the planar structure remains stable due to uniform SiO_2 coating, and the adsorption capacity increases, reaching a maximum of 2.57 mmol·g^{-1} at 7 wt% GO (GS7). In contrast, at higher GO contents (10-15 wt%), excessive GO leads to nanosheet agglomeration and non-uniform SiO_2 coating, which compromises planar structure stability and reduces the adsorption capacity to 1.74 mmol·g^{-1} at 15 wt% GO. In addition, PEI50-GS7 maintained 95.3% of its working capacity after 10 adsorption-desorption cycles, demonstrating good long-term stability, attributed to restricted PEI agglomeration by interlayer immobilization. For detailed characterization of the structure and surface properties, please refer to Supplementary Information (Figures S2-S10 & Table S1).

Microwave heating performance

Upon CO_2 adsorption, the amine sorbent was regenerated in a single-mode microwave device (Figure 1A). Figure 3 shows the microwave heating curves for different sorbents, where the temperature of the GO samples increased rapidly to 120°C within just 3 s at 10 W microwave power, highlighting its exceptional microwave absorption capacity. After compounding GO with SiO_2, the temperature of PEI50-GS sorbents rose to 102°C in 3 seconds, over 3 times faster than the 33°C achieved by PEI50-SiO_2. Such a difference in heating profile could be attributed to the higher ε'' (index of microwave-to-thermal conversion efficiency) of the PEI50-GS sample, for example, the ε'' for PEI50-GS7 and PEI50-SiO_2 was 0.22 and 0.12 at 2.45 GHz, respectively, higher than 2.89 and 0.12 for PEI50-SiO_2 (Figure S11). Notably, the heating rate of PEI50-GS7 ($\Delta T/\Delta t$ = 34 °C/s in the first 3 s) exceeded that of its GS7 support (28 °C/s), indicating a synergistic contribution of PEI loading in microwave heating. Though PEI50-GO achieved the fastest heating, its low CO_2 capacity (0.73 mmol·g^{-1} at 60°C) underscored the critical balance between dielectric response and CO_2 working capacity. Therefore, PEI50-GS7 struck an optimal balance between microwave responsiveness and CO_2 capture performance, making it a suitable candidate for the AS-MR process. In addition, the bulk density of sorbents plays a critical role in adsorption bed performance. The sorbent proposed in this work adopts a planar-stacked architecture, in which the sheet-like stacked microscopic morphology of GO endows the material with an ultralow bulk density of 0.1 g·cm^{-3}, which is far lower than that of conventional amine-based sorbents (PEI50/SiO_2: 0.5 g·cm^{-3}). This unique configuration effectively minimizes pressure drop across the packed bed and ensures a more uniform dielectric distribution throughout the sorbent layer, thereby offering distinct advantages over densely packed granular sorbents.

Dielectric properties (ε', ε'', and tan δ) of GO and PEI-GS sorbents with varying PEI loadings were analyzed (Figures S12-S13), showing that PEI50-GS sorbents with different GO ratios exhibited similar dielectric responses at approximately 2.4 GHz due to the low GO ratios at fixed PEI loading. The introduction of GO enhanced the microwave absorption capability of the sorbents at 2.4 GHz. Meanwhile, PEI loading effectively modulated the loss

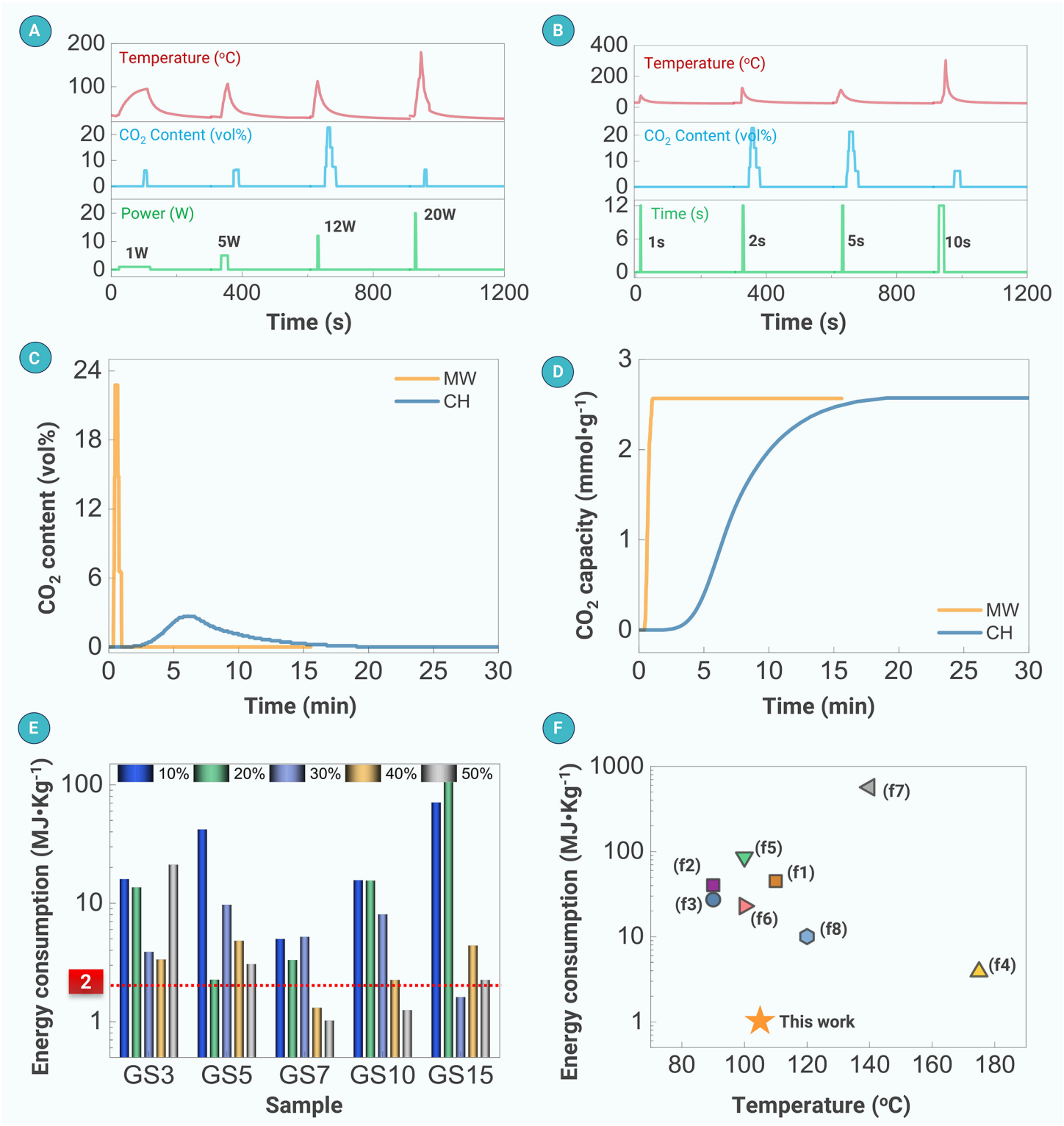

Figure 4. Microwave regeneration at different (A) power levels and (B) radiation durations. (C, D) Comparison of CO_2 release kinetics and capacity with microwave heating and conventional heating (CH). (E) Energy consumption of all sorbents in this work. (F) Comparison of energy consumption with reported work by microwave regeneration, including (f1) TETA/BDO,[31] (f2) MEA solution,[16] (f3) MEA/EG/PrOH,[32] (f4) 13X,[20] (f5) 30%MEA,[33] (f6) PZ,[34] (f7) MCM-48-tri,[35] and (f8) MGBIG.[36]

tangent (tan δ) of the composite through interfacial polarization. Specifically, increasing the PEI loading from 10 to 50 wt% raised tan δ from 0.05 to 0.07 (at 2.45 GHz), owing to enhanced dipole-dipole interactions between PEI and GS7. This increase in tan δ improved the microwave-to-thermal conversion efficiency from 62% to 81%, thereby directly accelerating CO_2 desorption kinetics. In addition, comparison with pure GO (tan δ = 0.11) and GS7 (tan δ = 0.06) highlights the synergistic dielectric behavior of the PEI50-GS7 composite.

AS-MR process by pulsed microwave

The microwave regeneration of PEI/GS sorbents was conducted under different power levels and durations. Before regeneration, all sorbents were exposed to 14 vol% CO_2 environments for 1 h at 60°C. Figure 4A shows the regeneration of PEI50-GS7 sorbent under 1, 5, 12, and 20 W. It took 94 s to gradually reach 94.8°C with 1 W input power. During this period,

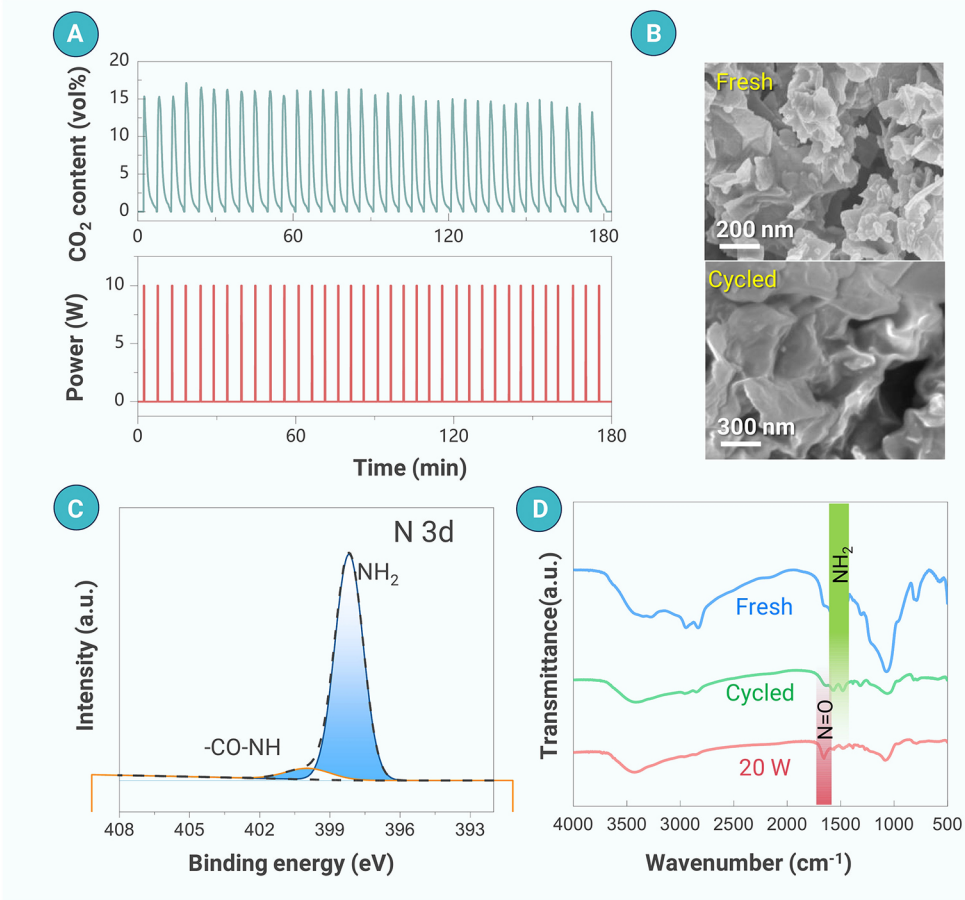

Figure 5. Stability assessment of the sorbent (A) Cycling performance of PEI50-GS7 under microwave heating at 12 W. (B) SEM image of fresh and 10 cycled PEI50-GS7. (C) XPS N 1s spectra of cycled PEI50-GS7. (D) FT-IR spectra of fresh, 10 cycled, and 20 W-irradiated PEI50-GS7.

0.48 mmol·g^{-1} of CO_2 was released, which was equivalent to 27% of the total amount adsorbed. The microwave power was further increased to 5 W, the sorbent reached 106.6°C in 19 s, yet only 28% of the adsorbed CO_2 was released. The incomplete desorption at low power was primarily attributed to insufficient energy input. Afterwards, by increasing the input power to 12 W, the sorbent temperature rapidly rose to 112.7°C within 2 s, resulting in complete desorption of the adsorbed CO_2.

However, further increasing the power to 20 W proved detrimental. With a 2 s pulse at 20 W, the sorbent temperature rapidly climbed to 180.0°C, but only 24% of the adsorbed CO_2 was released (Figure 4A). To understand this phenomenon, the sorbents were characterized by FT-IR spectroscopy before and after 20 W microwave irradiation. Compared to the fresh sorbent, a peak at 1654 cm^{-1} (C=O) was observed, suggesting the formation of a urea structure by reaction between amine and CO_2 due to thermal runaway at high input power (Figure 5D). Further tests were performed on PEI50-GS7 at the optimal input power of 12 W with different durations of 1, 2, 5, and 15 s (Figure 4B). Results showed that the sorbent temperature only reached 76.1°C during 1 s irradiation and no CO_2 was released, indicating that too-short microwave irradiation failed to provide sufficient energy for CO_2 desorption. Conversely, at a pulse duration of 15 s, thermal runaway occurred, similar to the scenario of 20 W for 2 s. These results suggested that using optimally powered pulsed microwave energy is essential for efficient CO_2 desorption and sorbent regeneration.

Figures 4C-D compares the regeneration process with PEI50-GS7 sorbent by using microwave irradiation and conventional heating. It took 2 min for microwave irradiation to reach complete regeneration, while over 10 min was needed for conventional heating. To calculate the energy consumption of the microwave process, the actual energy consumption (E_C) was measured and calculated using equations (1-2):

$$E_C = \frac{E_{abs}\,(MJ)}{q_{CO_2}\,(kg)} = \frac{\int_0^{t_{des}} P_{abs}(t)dt}{m \cdot q_{des}} \quad (1)$$

$$P_{abs} = P_{forward} - P_{reflected} \quad (2)$$

where q_{CO_2} is the amount of desorbed CO_2, P_{abs} is the difference between forward power and reflected power, and E_{abs} is absorbed energy by sorbents.

Among all tests, PEI40-GS7, PEI50-GS7, PEI50-GS10, and PEI30-GS15 exhibited the potential of reducing energy consumption to less than 2 MJ·kg^{-1}-CO_2, Figure 4E. The lowest value of 1.02 MJ·kg^{-1}-CO_2 was achieved in PEI50-GS7, attributing to its possession of both high CO_2 working capacity and excellent microwave absorption. This is the lowest value reported so far on microwave regeneration of amine sorbent.[37]

From the perspective of thermal thermodynamics, the ultrafast desorption kinetics (completed within 2 seconds) enabled by pulsed microwaves is fundamental to the observed energy efficiency. Unlike conventional amine solvent-based technologies, this process bypasses the substantial energy penalties associated with solvent evaporation (latent heat) and bulk solvent heating (sensible heat). Due to the selective dielectric interaction, microwave energy is precisely and instantaneously delivered to the polar amine-CO_2 interfaces to satisfy the endothermic enthalpy required for CO_2 dissociation. This targeted and rapid energy delivery ensures that desorption occurs before significant heat can propagate to the entire bulk sorbent or the environment, drastically suppressing parasitic sensible heat loss. On the other hand, TGA measurements (Section 1.6 of the Supplementary Information) estimated the total heat requirement for CO_2 desorption (encompassing sorbent sensible heat, CO_2 dissociation endothermy, and heat loss via gas flow) at 2.2 MJ·kg^{-1}. However, the microwave process achieved full regeneration with a total energy consumption of just 1.02 MJ·kg^{-1}-CO_2, merely 47% of the thermodynamic minimum required for conventional thermal desorption. This efficiency, surpassing theoretical limits of bulk heating, confirms the presence of microwave-specific non-thermal effects: microwaves induce localized dipolar excitation at amine-CO_2 binding sites, facilitating direct cleavage of CO_2-NH bonds.[38] A detailed comparison of energy consumption under microwave heating is presented in the Supporting Information (Table S2 & Figures S14-S19).

To evaluate the long-term stability, PEI50-GS7 was tested for 10 cycles of adsorption and microwave desorption continuously. The sorbent retained the same working capacity during the 35-cycle tests (Figure 5A). Characterization results further confirmed the well-remained morphological (Figure 5B) and chemical features (Figures 5C-D) after cycling tests. Especially, by analyzing the N1s signal from XPS results, $I_{H\text{-}N\text{-}C}/I_{N\text{-}H}$ ratio was not changed, indicating that the amine groups remained unchanged after microwave irradiation. No urea peak was observed in FT-IR spectra, suggesting a reversible process with appropriate control of energy input by pulsed microwave.

Mechanism of microwave regeneration

To understand the mechanism of microwave-assisted CO_2 desorption, density functional theory (DFT) calculations were performed using external electric fields (EFs) as equivalents of microwave fields, as derived from Maxwell's equations. For a detailed analysis of the EFs' impact on structural configurations and electron cloud distributions, refer to the Supporting Information. Briefly, the desorption pathway moved from a chemisorbed carbamate acid (CA) through a transition state (TS) to a physisorbed CO_2 state

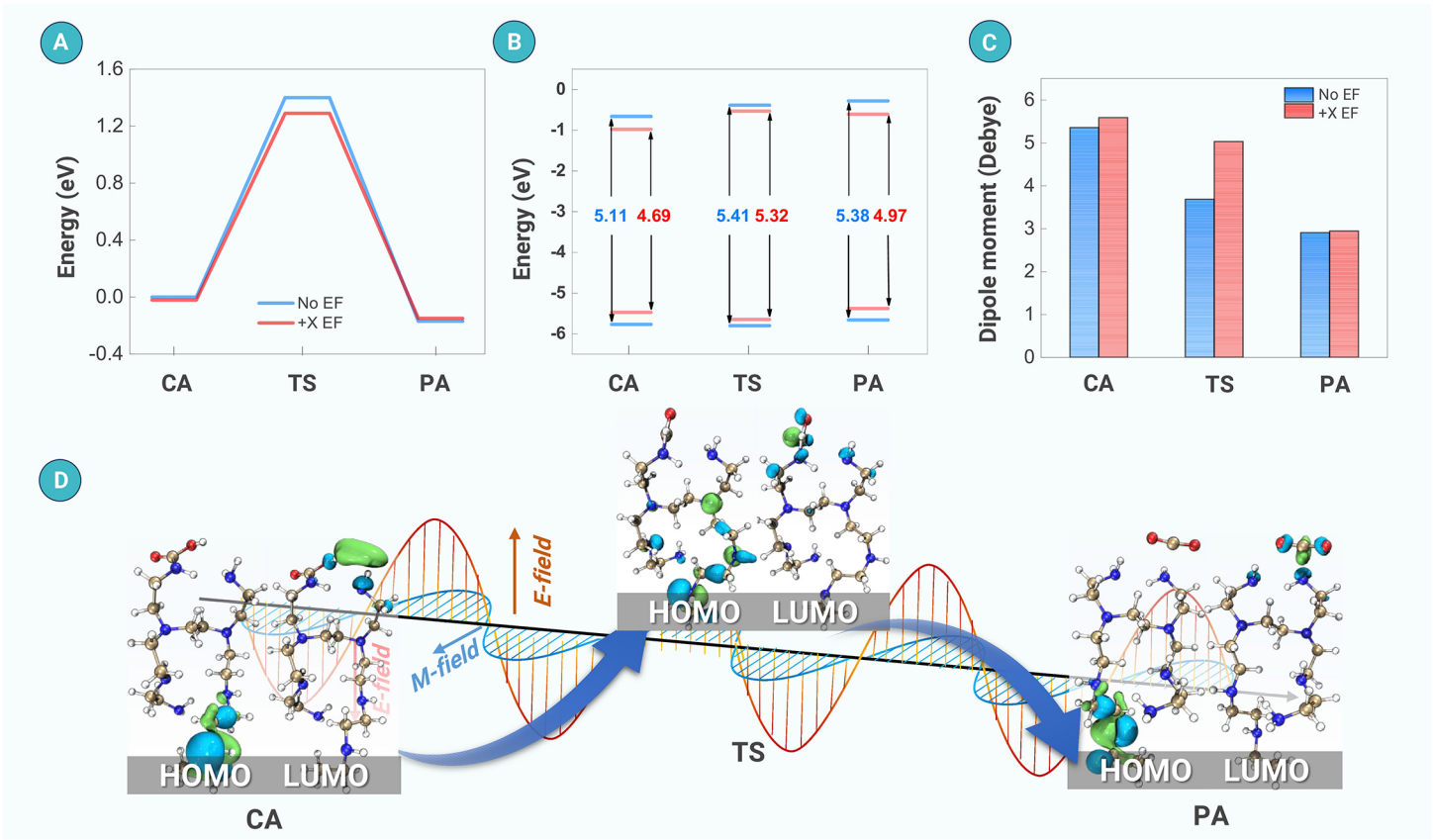

Figure 6. The DFT calculation of microwave regeneration (A) Total energy. (B) Molecular orbital energy levels. (C) Dipole moment of CA, TS and PA varies with +X direction electric field (intensity E = 0.001 a.u.). (D) FMOs visualization (isovalue = 0.05, blue/green region: +/- phases, red atom: O, white atom: H, brown atom: C, blue atom: N) and scheme of microwave effect.

(PA), necessitating the overcoming of an activation energy barrier of 1.40 eV (Figure 6A). By applying EFs from 6 different directions, results (Figures S20-S22 & Table S3) indicated that these EFs, particularly along +X and +Z axes, substantially lowered the desorption activation barrier (e.g., by 0.10 eV to 1.30 eV for +X EF).

There was a strong correlation between the reduction in barrier and increased charge transfer (Δ_{TS}) from the amine nitrogen to the CO_2 carbon at the TS state. For instance, under a +X EF, the Δ_{TS} increased from -0.314 to -0.330 e, facilitating the breaking of the C-N bond. EFs that lowered the barrier also corresponded to a slightly shorter C-N bond length at the TS, suggesting that the TS was structurally closer to CA. Additionally, the +X, Z, and +Y EFs altered the desorption energy difference (E_{PA} - E_{CA}), for instance, reducing it from 0.17 eV to 0.13 eV under the +X EF. This indicated that directional EFs induced structural changes between the adsorbed and desorbed states, resulting in a reduction in adsorption energy. These findings demonstrated that directional EFs enhanced CO_2 desorption by reducing desorption energy barriers.

Frontier molecular orbital (FMO) analysis reveals electronic changes across the desorption states, as shown in Figure 6B. In the absence of an EF, CA exhibits a HOMO- LUMO gap of 5.11 eV, with the LUMO localized on the NH_2-CO_2 part, particularly the π* antibonding orbitals of the C=O bonds and the carbamate carbon, reflecting CO_2's electrophilicity. The TS, with a gap of 5.41 eV, shows the LUMO centered on the detaching CO_2, while PA, with a gap of 5.38 eV, has the LUMO almost entirely on the desorbed CO_2, reflecting its independent electronic structure post-desorption. The +X EF alters the electron distribution of HOMO, reducing the HOMO-LUMO gap across all states (CA, TS and PA). It indicated that +X EF stabilized the LUMO and destabilized the HOMO, which collectively facilitate electron transfer and enhance the system's reactivity. The observed redistribution of electron density under the electric field has profound implications for the CO_2 desorption process, particularly at the TS.

The HOMO of the TS shifts toward the +X direction, concentrating electron density at the reaction center (Figure S23 & Table S4). Concurrently, the LUMO exhibits intensified green regions localized on the CO_2 carbon atom, with slightly diminished blue regions on the oxygen atoms. This indicates stronger LUMO localization on CO_2, amplifying antibonding interactions that promote C-N bond cleavage. These synergistic changes in HOMO and LUMO distributions lower the energetic barrier for CO_2 release. In the PA, the EF induces a more compact electron cloud around the nitrogen atom, signifying stabilization of electron density on the amine group. Simultaneously, the LUMO's antibonding regions become more diffuse, weakening antibonding character and reducing the PA's electron affinity. This stabilizes the product configuration, preventing undesired back-reactions. These electronic rearrangements align with the observed reduction in reaction barrier and increased charge transfer (Figures S24-S25), demonstrating that a directionally applied EF effectively enhances the CO_2 desorption process by modulating orbital interactions critical to C-N bond cleavage.

Dipole moment calculations provided additional insight into the EF's polarizing effects (Figure 6C). Without an EF, dipole moments for CA, TS, and PA were 5.3572, 3.6866, and 2.9100 debye, respectively; under +X EF, these values increased to 5.5904, 5.0304, and 2.9464 debye. It was worth noting that the TS exhibited a pronounced increase, reflecting enhanced charge separation that stabilized the polar TS and aided C-N bond cleavage; the PA state showed minimal change, indicating the negligible influence of EF on the PA state. This equation (S3) reveals that permittivity (and thus microwave responsiveness) increases with the square of the dipole moment. Consequently, the significant increase in TS dipole moment under +X EF (from 3.6866 to 5.0304 debye) directly enhances its permittivity, strengthening its ability to absorb microwave energy. This amplified microwave response accelerates the conversion of TS to the PA state (which maintains a low dipole moment and weak microwave interaction), thereby promoting rapid CO_2 desorption. Additional dipole moment data and derivations are provided in the Supplementary Information. Together, these findings demonstrated that microwave fields enhanced CO_2 desorption

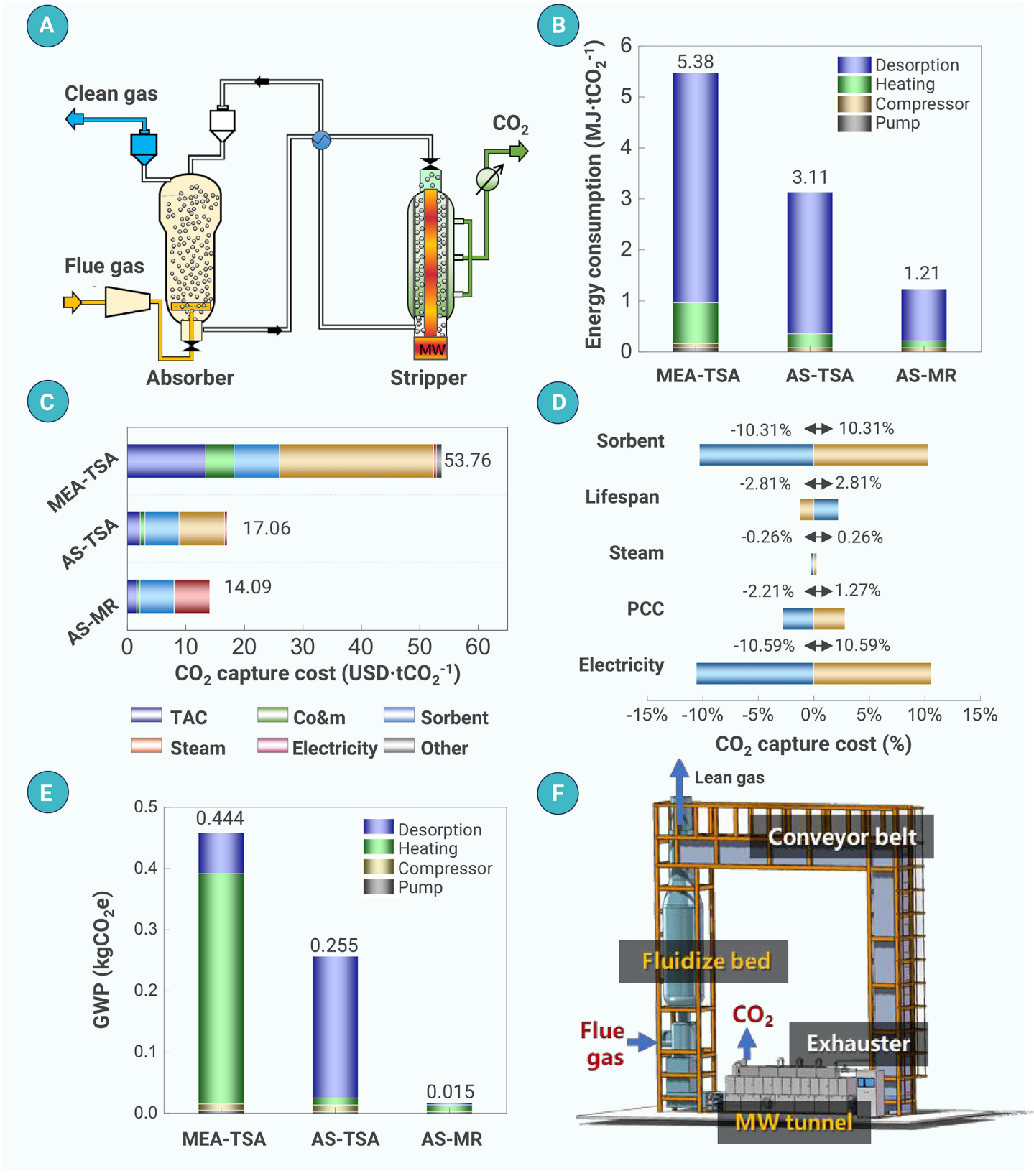

Figure 7. Comparison of three CO_2 capture technologies: MEA-TSA, AS-TSA, and AS-MR. (A) Flowchart of the AS-MR process. (B) CO_2 capture energy consumption. (C) CO_2-avoidance cost. (D) Sensitivity analysis of CO_2-avoidance cost in AS-MR process. (E) CO_2 capture carbon footprint. (F) Conceptual design of pilot-scale demonstration.

from PEI via a synergistic electronic mechanism: (1) weakening and polarizing the C-N bond in the CA state, and (2) stabilizing the TS by altering frontier orbital energies and increasing charge separation. This dual modulation highlighted the promise of electrically-assisted sorbent regeneration for amine-based CO_2 capture systems, providing a pathway to improve desorption efficiency.

Techno-economic analysis and life cycle assessment

TEA and LCA are vital steps for evaluating the economic viability and carbon emission reduction potential of the microwave-assisted CO_2 capture

process. In this work, three processes were modeled: the amine scrubbing system with TSA (MEA-TSA), the amine sorbent-based system with TSA (AS-TSA), and the AS-MR. Figure 7A illustrates the AS-MR process, including an absorber, microwave stripper, compressor, cyclone separator, and heat exchanger. The process designs of the MEA-TSA process and the solid amine capture processes (AS-TSA and AS-MR) were illustrated in Figures S26-S29, respectively. Detailed methods and assumptions are provided in Tables S5-S6. Figure 7B indicated that the overall energy consumption of MEA-TSA was 5.38 MJ·kg^{-1} CO_2, consistent with reported values in the range of 4-6 MJ·kg^{-1} CO_2.[26] The energy consumption of the AS-TSA decreased to 3.11 MJ·kg^{-1} CO_2, primarily due to the reduction of sensible heat of solvent and the lower enthalpy of desorption (Table S7). The AS-MR process further lowered energy consumption to 1.21 MJ·kg^{-1} CO_2, successfully achieving the US DOE energy goal of 2.0 MJ·kg^{-1} CO_2 by 2035. The key difference of these processes was the energy transfer mode; microwaves delivered energy directly to the sorbent, allowing for more effective utilization of energy for CO_2 desorption. In addition, Table S8 compared the energy consumption of various CO_2 capture technologies.

The CO_2-avoidance costs of MEA-based solvents were substantial, reaching 53.76 USD·tonne^{-1} CO_2 (Figure 7C). The economic analysis assumptions are provided in Tables S9-S10. The regeneration of spent amine solution with hot pressurized steam at 120-140°C and 1-2 bar, and considerable amine degradation were the main cost factors during operation. Moreover, the lengthy regeneration time[39] led to large equipment size and capital expenses. AS-TSA and AS-MR processes were more cost-effective, with costs of 17.06 and 14.09 USD·tonne^{-1} CO_2, respectively, compared to MEA-TSA. This was mainly due to lower capital expenditures, resulting from a simpler procedure and smaller plant size, as well as reduced maintenance and material costs. It was worth noting that industrial microwave devices have been used in a variety of industrial processes, and the capital cost of microwave devices is unlikely to rise significantly compared to the new steam reboiler. Figures 7D & S30 showed a sensitivity analysis of the key factors affecting CO_2-avoidance costs, assessing the impact of a 25% increase and decrease for each parameter. The results indicated that energy prices (both electricity and steam) exerted a remarkable influence on the CO_2-avoidance costs across all three processes. Notably, as renewable energy advanced and the electricity price dropped to 0.02 USD·kWh^{-1},[40] microwave desorption powered by renewable electricity became more economically advantageous compared to the steam regeneration using fossil fuels. The results of the economic analysis for the three scenarios are presented in Table S11. In addition, the production cost of the sorbent was further analyzed. For large-scale production, the estimated material cost ranges from 5500 to 9700 USD per tonne, based on fixed industrial unit prices of TEOS, GO, and PEI and variable material loadings in the synthesis process (Table S12). Moreover, scalable synthesis strategies, such as continuous spray drying for nanosheet-based composites, were proposed to further reduce production cost and improve process uniformity, indicating the strong scalability and industrial feasibility of the synthesis route.

LCA further highlighted the effective emission reduction potential of AS-MR (Figure 7E). The MEA-TSA process exhibited a relatively high global warming potential (GWP) of 0.444 kgCO_2e. This indicated that capturing 1 kg of CO_2 resulted in an additional 0.444 kgCO_2e of emissions, leading to a net reduction of only 0.566 kgCO_2e. Previous studies have reported that the GWP of the MEA-TSA process was not sustainable for CO_2 capture technology, with values ranging from 0.200 to 0.600 kgCO_2e.[41–42] Thus, achieving a higher net carbon reduction is a critical metric for evaluating CO_2 capture technologies. In this work, the AS-MR process demonstrated a significantly lower GWP, emitting only 0.015 kgCO_2e per 1 kg of CO_2 captured (Figure 7D). This was primarily attributed to the utilization of green electricity to power the AS-MR process. As green electricity technologies advanced, the GWP associated with the AS-MR process was expected to decline further.

Based on the aforementioned TEA and LCA, a pilot-scale demonstration for the AS-MR process was designed to capture 200 m^3·h^{-1}, as depicted in Figure 7F. The design allowed the sorbent to adsorb CO_2 in a fluidized bed that was 4 m high. The clean gas was then discharged through a cyclone separator. The CO_2-rich sorbent moved downward to the 2 m-long microwave tunnels for pulsed microwave regeneration. An industrial-scale microwave tunnel equipped with conveyor belts was utilized for solid sorbent regeneration. At the top of the microwave tunnel, the desorbed CO_2 was extracted and compressed for downstream applications. Finally, the sorbent was conveyed back to the fluidized bed for the next adsorption cycle. This size reduction allowed for a more compact deployment configuration compared to existing pilot-scale amine scrubbing processes.

CONCLUSION

In summary, we developed an AS-MR process that enabled low-energy consumption CO_2 capture by integrating microwave-responsive amine sorbents (PEI-GS) with a pulsed microwave-assisted regeneration system. The targeted microwave irradiation to control both energy transfer and CO_2 desorption was aligned to achieve a remarkable CO_2 desorption rate, in just 2 seconds, and reducing energy consumption to 1.02 MJ·kg^{-1} CO_2. This highly efficient regeneration rate was ten times faster than that of conventional regeneration. Furthermore, the systematic assessment of AS-MR demonstrated that the overall energy consumption is 1.21 MJ·kg^{-1} CO_2. The TEA indicated that the cost of CO_2 avoidance is merely 14.09 USD·tonne^{-1} CO_2, significantly less than that of currently reported carbon capture technologies. Mechanism study revealed that directional EFs enhance CO_2 desorption by reducing the activation energy barrier for C-N bond cleavage (from 1.40 eV to 1.30 eV under +X EF) through increased charge transfer from amine nitrogen to CO_2 carbon at the transition state, narrowing HOMO-LUMO gaps, and enhancing the polarization of carbamate state. This work presents an ultrafast and ultra-low-energy carbon capture technology, which provides a transformative means for capturing CO_2 within an economically viable range.

REFERENCES

1. Service R. F. (2021). Carbon capture marches toward practical use. *Science* **371**:1300. DOI:10.1126/science.371.6536.1300
2. Li S., Feng Y., Li Y., et al. (2024). Critical review on mobile direct air capture: Concept expansion, characteristic description, and performance evaluation. *Matter* **7**:889–933. DOI:10.1016/j.matt.2024.01.003
3. Meinshausen M., Lewis J., McGlade C., et al. (2022). Realization of Paris agreement pledges may limit warming just below 2 °C. *Nature* **604**:304. DOI:10.1038/s41586-022-04553-z
4. Rochelle G. T. (2009). Amine scrubbing for CO_2 capture. *Science* **325**:1652–1654. DOI:10.1126/science.1176731
5. Min K., Choi W., Kim C., et al. (2018). Oxidation-stable amine-containing adsorbents for carbon dioxide capture. *Nat. Commun.* **9**:726. DOI:10.1038/s41467-018-03123-0
6. Aghel B., Janati S., Wongwises S., et al. (2022). Review on CO_2 capture by blended amine solutions. *Int. J. Greenhouse Gas Control* **119**:103715. DOI:10.1016/j.ijggc.2022.103715
7. Zhao F., Cui C., Dong S., et al. (2023). An overview on the corrosion mechanisms and inhibition techniques for amine-based post-combustion carbon capture process. *Sep. Purif. Technol.* **304**:122091. DOI:10.1016/j.seppur.2022.122091
8. Zhou T., Wen Y., Wu Z., et al. (2024). Dual-bonded polyethyleneimine network with electron-withdrawing groups at α, β-sites for ultra-stable and low-energy CO_2 capture in harsh environments. *Green Energy Environ.* **10**:1039–1049. DOI:10.1016/j.gee.2024.10.005
9. Zhou T., Wu Z., Wen Y., et al. (2024). Networking SiO_2-Al_2O_3 and amines into robust and long-lasting molded sorbents for continuous CO_2 capture. *Chem. Eng. J.* **499**:156446. DOI:10.1016/j.cej.2024.156446
10. Siegelman R. L., Kim E. J. and Long J. R. (2021). Porous materials for carbon dioxide separations. *Nat. Mater.* **20**:1060–1072. DOI:10.1038/s41563-021-01054-8
11. Naeem M. A., Armutlulu A., Imtiaz Q., et al. (2018). Optimization of the structural characteristics of CaO and its effective stabilization yield high-capacity CO_2 sorbents. *Nat. Commun.* **9**:2408. DOI:10.1038/s41467-018-04794-5
12. Yoo C.-J., Park S. J. and Jones C. W. (2020). CO_2 adsorption and oxidative degradation of silica-supported branched and linear aminosilanes. *Ind. Eng. Chem. Res.* **59**:7061–7071. DOI:10.1021/acs.iecr.9b04205
13. Liu H., Wang X., Chen S., et al. (2024). Sponge-like polyethyleneimine adsorbents with interconnected open channels enabling ultra-high CO_2 adsorption and separation capacity. *Sep. Purif. Technol.* **330**:125528. DOI:10.1016/j.seppur.2023.125528
14. Lai Q., Toan S., Assiri M. A., et al. (2018). Catalyst-$TiO(OH)_2$ could drastically reduce the energy consumption of CO_2 capture. *Nat. Commun.* **9**:2672. DOI:10.1038/s41467-018-05145-0
15. Ai Y., Xing R., Ren N., et al. (2025). Biomass-derived hierarchical carbon frameworks enable robust microwave absorption. *Matter* **8**:102289. DOI:10.1016/j.matt.2025.102289
16. Bougie F. and Fan X. (2018). Microwave regeneration of monoethanolamine aqueous solutions used for CO_2 capture. *Int. J. Greenhouse Gas Control* **79**:165–172. DOI:10.1016/j.ijggc.2018.10.008

17. McGurk S. J., Martin C. F., Brandani S., et al. (2017). Microwave swing regeneration of aqueous monoethanolamine for post-crossmark combustion CO_2 capture. *Appl. Energy* **192**:126–133. DOI:10.1016/j.apenergy.2017.02.012
18. Gomez-Rueda Y., Verougstraete B., Ranga C., et al. (2022). Rapid temperature swing adsorption using microwave regeneration for carbon capture. *Chem. Eng. J.* **446**:137345. DOI:10.1016/j.cej.2022.137345
19. Yang J., Tan H. Y., Low Q. X., et al. (2015). CO_2 capture by dry alkanolamines and an efficient microwave regeneration process. *J. Mater. Chem. A* **3**:6440–6446. DOI:10.1039/c4ta06273f
20. Erguvan M. and Amini S. (2024). Experimental microwave assisted CO_2 desorption of a solid sorbent in a fluidized bed reactor. *Sep. Purif. Technol.* **343**:127062. DOI:10.1016/j.seppur.2024.127062
21. Qi G., Fu, L., Choi B. H., et al. (2012). Efficient CO_2 sorbents based on silica foam with ultra-large mesopores. *Energy Environ. Sci.* **5**:7368–7375. DOI:10.1039/C2EE21394J
22. Frisch M. J., Trucks G. W., Schlegel H. B., et al. (2016). Gaussian, Version 16, Revision A. 03; Gaussian. *Inc.: Wallingford, CT, USA*. https://gaussian.com/relnotes_a03/
23. Becke, A. D. (1993). Density - functional thermochemistry. III. The role of exact exchange. *J. Chem. Phys.* **98**:5648–5652. DOI:10.1063/1.464913
24. Grimme S., Antony J., Ehrlich S., et al. (2010). A consistent and accurate ab initio parametrization of density functional dispersion correction (DFT-D) for the 94 elements H-Pu. *J. Chem. Phys.* **132**:154104. DOI:10.1063/1.3382344
25. Hariharan P. C. and Pople J. A. (1973). The influence of polarization functions on molecular orbital hydrogenation energies. *Theor. Chim. Acta* **28**:213–222. DOI:10.1007/BF00533485
26. Yang F., Meerman J. and Faaij A. (2021). Carbon capture and biomass in industry: A techno-economic analysis and comparison of negative emission options. *Renewable Sustainable Energy Rev.* **144**:111028. DOI:10.1016/j.rser.2021.111028
27. Mevawala C., Bai X., Hu J., et al. (2023). Plant-wide modeling and techno-economic analysis of a direct non-oxidative methane dehydroaromatization process via conventional and microwave-assisted catalysis. *Appl. Energy* **336**:120795. DOI:10.1016/j.apenergy.2023.120795
28. Jiao X., Qiu Y., Zhang L., et al. (2017). Comparison of the characteristic properties of reduced graphene oxides synthesized from natural graphites with different graphitization degrees. *RSC Adv.* **7**:52337–52344. DOI:10.1039/c7ra10809e
29. Wang M., Ma L., Li B., et al. (2020). One-step generation of silica particles onto graphene oxide sheets for superior mechanical properties of epoxy composite and scale application. *Compos. Commun.* **22**:100514. DOI:10.1016/j.coco.2020.100514
30. Guo Y., Luo L., Zheng Y., et al. (2020). Optimization of CO_2 adsorption on solid-supported amines and thermal regeneration mode comparison. *ACS Omega* **5**:9641–9648. DOI:10.1021/acsomega.9b03374
31. Li Y., Gao J., Li J., et al. (2020). Screening and performance evaluation of triethylenetetramine nonaqueous solutions for CO_2 capture with microwave regeneration. *Energy Fuels* **34**:11270–11281. DOI:10.1021/acs.energyfuels.0c02006
32. Bougie F., Pokras D. and Fan X. (2019). Novel non-aqueous MEA solutions for CO_2 capture. *Int. J. Greenhouse Gas Control* **86**:34–42. DOI:10.1016/j.ijggc.2019.04.013
33. Balraj A., Premalalitha P. P., Ramamoorthy S. V., et al. (2022). Experimental investigation of microwave-assisted regeneration of carbon-rich aqueous solutions. *Chem Eng. Process.* **177**:109000. DOI:10.1016/j.cep.2022.109000
34. Premalalitha P. P. and Balraj A. (2024). Low-temperature dielectric heating-assisted CO_2 stripping/solvent regeneration of aqueous carbon-rich monoethanolamine, piperazine, and 2-amino-2-methyl-1-propanol solvents. *Ind. Eng. Chem. Res.* **63**:1975–1987. DOI:10.1021/acs.iecr.3c03671
35. Nigar H., Garcia-Banos B., P enaranda-Foix F. L., et al. (2016). Amine-functionalized mesoporous silica: A material capable of CO_2 adsorption and fast regeneration by microwave heating. *AIChE J.* **62**:547–555. DOI:10.1002/aic.15118. DOI:10.1002/aic.15118
36. Jang G. G., Kasturi A., Stamberga D., et al. (2023). Ultra-fast microwave regeneration of CO_2 solid sorbents for energy-efficient direct air capture. *Sep. Purif. Technol.* **309**:123053. DOI:10.1016/j.seppur.2022.123053
37. Wu Y., Chen X., Ma J., et al. (2020). System integration for coal-fired power plant with post combustion CO_2 capture: Comparative study for different solid dry sorbents. *Fuel* **280**:118561. DOI:10.1016/j.fuel.2020.118561
38. Tao Y., Teng C., Musho T. D., et al. (2021). Direct measurement of the selective microwave-induced heating of agglomerates of dipolar molecules: the origin of and parameters controlling a microwave specific superheating effect. *J. Phys. Chem. B* **125**:2146–2156. DOI:10.1021/acs.jpcb.0c10291
39. Jaffar M., Brandoni C., Martinez J., et al. (2023). Comparative techno-economic analysis of the integration of MEA-based scrubbing and silica PEI adsorbent-based CO2 capture processes into cement plants. *J. Cleaner Prod.* **414**:137666. DOI:10.1016/j.jclepro.2023.137666
40. De Luna P., Hahn C., Higgins D., et al. (2019). What would it take for renewably powered electrosynthesis to displace petrochemical processes. *Science* **364**:eaav3506. DOI:10.1126/science.aav3506
41. Grant T., Anderson C. and Hooper B. (2014). Comparative life cycle assessment of potassium carbonate and monoethanolamine solvents for CO_2 capture from post combustion flue gases. *Int. J. Greenhouse Gas Control* **28**:35–44. DOI:10.1016/j.ijggc.2014.06.020
42. von der Assen N., Voll P., Peters M., et al. (2014). Life cycle assessment of CO_2 capture and utilization: a tutorial review. *Chem. Soc. Rev.* **43**:7982–7994. DOI:10.1039/C3CS60373C

FUNDING AND ACKNOWLEDGMENTS

The authors appreciate the financial support from the National Key Research and Development Program of China (No. 2024YFE0206200), the National Natural Science Foundation of China (No. 22378183, 22378184, and 22408155), and the Natural Science Foundation of Jiangsu Province, China (No. BK20230328). The funders had no role in study design, data collection and analysis, decision to publish, or preparation of the manuscript.

AUTHOR CONTRIBUTIONS

Y.X. Wen and P. Jiang contributed equally to this work. All authors contributed to the manuscript and approved the final version.

DECLARATION OF INTERESTS

The authors declare no competing interests.

DATA AND CODE AVAILABILITY

The authors declare that the main data supporting the findings of this study aro available within the paper and its Supplemental Information. Extra data are available on reasonable request from the corresponding author.

SUPPLEMENTAL INFORMATION

It can be found online at https://doi.org/10.59717/j.xinn-mater.2026.100224.